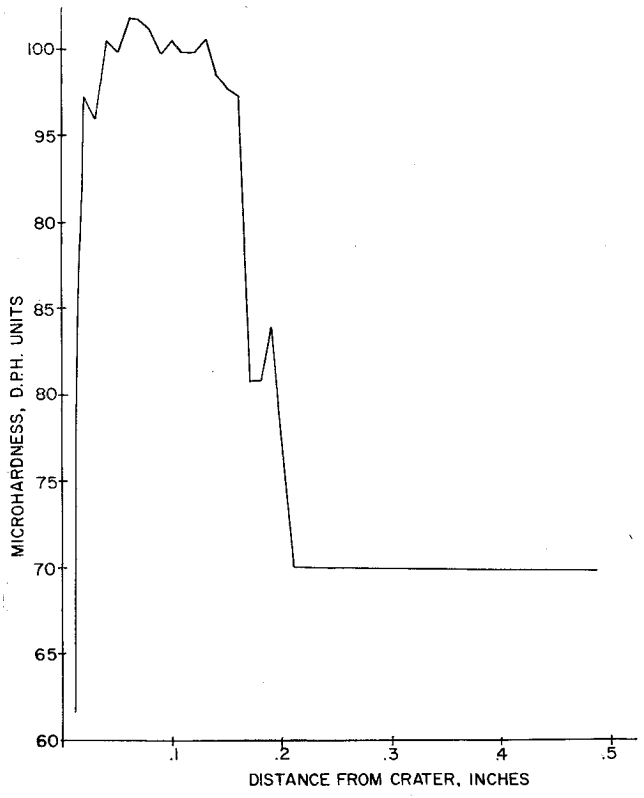


**Fig. 5 Microhardness as a function of radial distance from crater.**

higher hardness indicative of strain hardening without recrystallization.

Measurements of hardness on the heated targets indicate a more general softening around the crater, the depth of softening away from the crater being greater than in the case of the unheated targets. However, even the heated targets showed a very thin layer near the crater which was considerably softer than the material more removed from the crater.

### Conclusion

It is concluded that there is an exact correlation between temperature and yield strength. The crater volume is seen to be dependent on the $-0.396$ power of the yield strength for impacts of aluminum spheres on semi-infinite aluminum targets in the velocity range from 12,700 to 21,750 fps. From a transition point, at about 13,000 fps and up to at least 21,750 fps, the crater volume is not dependent on the kinetic energy of the projectile but rather on the velocity to the 1.78 power, indicating that the strength effect on the cratering process may be diminishing above a velocity of 13,000 fps. Microhardness readings seem to indicate that sufficient heat was generated during the impact to cause recrystallization in a thin layer, estimated to be 0.015 in. thick at the bottom of the crater.

### References

[1] Ferguson, W. J. and McKinney, K. R., "The influence of temperature elevation on the penetration of missiles in copper targets," Naval Research Lab. Rept. 5407 (November 1959).

[2] Allison, F. E., Becker, K. R., and Vitali, R., "Effects of target temperature on hypervelocity cratering," Fourth Hypervelocity Impact Symposium, Vol. 1 (April 1960).

[3] Rockowitz, R., Carey, C. A., and Dignam, J. F., "Hypervelocity impact of heated copper," Fifth Symposium on Hypervelocity Impact, Vol. 1 (April 1962).

[4] Bjork, R. L., "Effects of a meteoroid impact on steel and aluminum in space," TR P-1662, Rand Corp., Engineering Div. (December 1958).

# Longitudinal Wave Propagation in Liquid Propellant Rocket Motors

Sanford S. Hammer* and Vito D. Agosta†
*Polytechnic Institute of Brooklyn, Farmingdale, N. Y.*

### Introduction

Longitudinal wave propagation studies are being conducted in a liquid propellant rocket motor in order to define the parameters that determine whether an input disturbance will attenuate or amplify. Since combustion instability is a measure of the relative amounts of energy accumulation in a cavity in contradistinction to the energy dissipation from the cavity, the mechanisms that allow such behavior should be analyzed in detail. Particular emphasis must be placed upon the interaction of pressure waves and the fluid dynamic field.

Consider the case where the relaxation times of significant processes are in excess of the wave residence time in a volume element of a liquid propellant rocket motor. It can be envisaged that the toe of a passing wave in a reacting droplet system can increase the rate of evaporation, which couples as a mass source to the heel of a passing wave, thus producing amplification. It can further be seen that, for a long relaxation time, the mass source can generate wavelets that coalesce as they propagate and ultimately overtake the initial wave that caused the disturbance, thereby causing amplification. In addition, as a wave propagates in a gas, it deforms. A compression wave will steepen in a decelerating flow; an expansion wave will broaden in an accelerating flow. A compression wave in an accelerating flow and an expansion wave in a decelerating flow will either broaden or steepen, depending on the wave slope and the velocity gradient of the gaseous medium. Therefore, as a wave moves in a rocket chamber, it will change its geometry, which then alters its residence time in a volume element. In addition, the energy in a wave is a function of its velocity and waveform. Thus, the wave slope assumes a major role in that it determines, by modifying the effective wavelength and amplitude, the nature of the energy or mass coupling to the propagating wave and the ultimate stability of the system.

This note presents some recent experimental data on wave-shape behavior in a liquid rocket motor in addition to measurements of the effect of Mach number on the frequency of wave propagation.

### Experimental Equipment

Experiments are being conducted in a 2-in.-diam 500-lbf nominal thrust, JP-5A-Lox rocket motor. The injector is of the shower-head type with 16 fuel and 16 oxidizer orifices. The total propellant flow is 2.37 lbm/sec at an oxidizer-fuel ratio of 2.79. The chamber length is 22.5 in. measured from the injector face to the start of the converging nozzle. The nozzle contraction ratio is 1.5, resulting in a high Mach number profile through the chamber. High frequency-response pressure transducers (Photocon model no. 352) are flush-mounted in the chamber at 3, 13, and 21 in. from the injector face. Data are recorded on magnetic tape at 60 in./sec and played back at 1 in./sec into a recording oscillograph with a paper speed of 25 in./sec. Approximately

Received June 30, 1964. The results presented in this paper were obtained in the course of research sponsored by the Air Force Office of Scientific Research under Contract AF 49(638)-1263. The authors wish to acknowledge William T. Peschke for his valuable assistance in the performance of the tests in this investigation.

* Research Associate, Aerospace Engineering, Propulsion Research Laboratory. Member AIAA.

† Professor of Aerospace Engineering, Propulsion Research Laboratory. Member AIAA.

6 sec after startup (steady-state chamber pressure is 165 psia measured 3 in. from the injector face), the wave generator tube diaphragm is ruptured, and a wave propagates into the rocket motor thrust chamber. The wave generator is actually a modified shock driver tube mounted axially through the injector manifold and utilizing the rocket motor combustor as the driven tube. The transition piece between the shock driver tube and the combustor shapes the input wave. The diaphragm is in a plane parallel to the injector face. Diaphragm rupture is accomplished with a solenoid actuated needle. The wave generator tube driver pressure is 725 psia.

### Results and Discussion

A diagram showing the time of arrival of the wave at the various transducer locations is shown in Fig. 1, along with the tabulation of various parameters. The initial wave is generated with a wave slope of 32 psi/in. As the wave propagates through the combustion zone, i.e., between 3 and 10 in. from the injector face, where large longitudinal pressure and velocity gradients are present, it is seen to broaden. Actual transducer outputs from the 3- and 13-in. locations reveal a train of secondary wavelets following behind the initial input wave (Fig. 2a). The pressure history at the 21-in. transducer indicates that all of the secondary waves have coalesced with the initial wave to form a single steepening wave. The secondary wavelets have a frequency well below that expected for either a tangential or radial mode and are therefore presumed to be due to the passage of the longitudinal wave through the evaporation zone. The wave causes a shattering of drops with an attendant increase in over-all evaporation and combustion rates. Since the steady-state work[1, 2] has previously shown the evaporation and combustion zone to be limited to the first 10 to 12 in. of chamber for the injector currently in use, it would not be expected that combustion waves be produced in the latter half of the chamber. It is interesting to note, however, that the secondary or combustion waves produced in the upstream portion of the chamber coalesce into the incident wave before arrival at the 21-in. transducer.

The wave that is reflected upstream from the nozzle end is initially attenuated. However, as it propagates upstream, it steepens considerably (from 17 to 105 psi/in.). An extrapolation of the wave diagram for the incident and reflected wave indicates that the equivalent reflecting surface is exactly coincident with the sonic plane at the nozzle throat.

At the injector face, the wave is reflected and starts a second traverse of the chamber. In all, three complete cycles are required before the steady-state component of the pressure is reduced to the prewave value. The maximum pressures are recorded behind the first reflection from the nozzle.

After the input disturbance has dissipated to a point where the steady-state chamber pressure has assumed its prewave

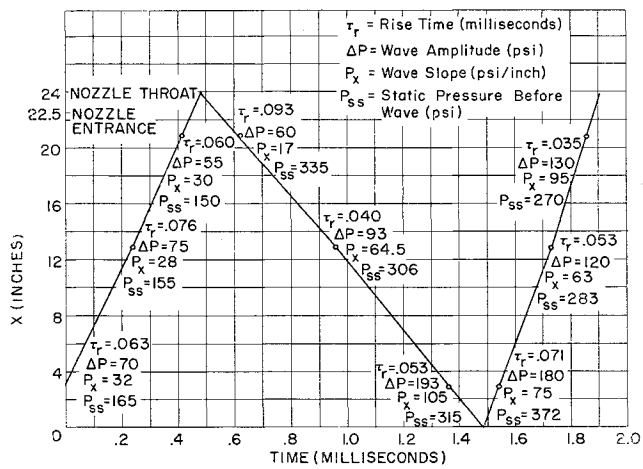


**Fig. 1 Properties of initial wave.**

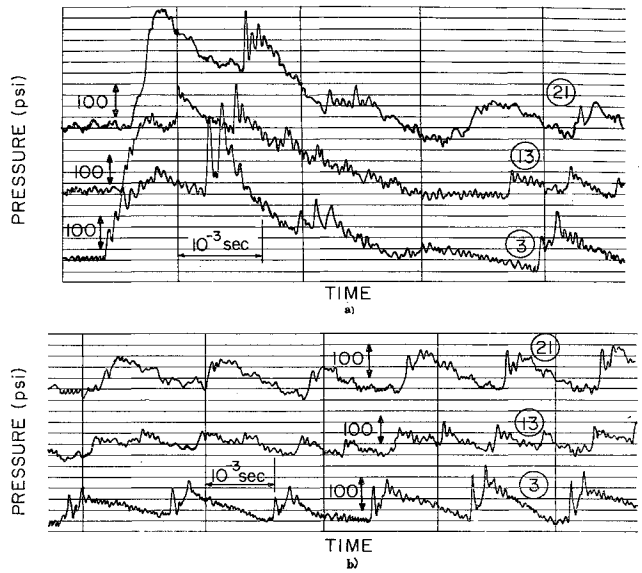


**Fig. 2 a) Pressure vs time for initial wave; and b) pressure vs time for initiated oscillations.**

value, a second type of wave propagation is detected. The output of all transducers indicates a periodic disturbance propagating longitudinally in the thrust chamber (Fig. 2b). The wave is initiated at the injector face, propagates downstream, reflects from the sonic plane of the nozzle throat, and propagates upstream. At the injector face, the wave is reflected once more and travels toward the nozzle. The period of the disturbance (defined as the time between two successive waves traveling in the same direction) is 1.37 msec. The amplitude of the overpressure is approximately 100 psi with a rise time of 0.05 msec. The pressure decays behind each incident wave to the steady-state chamber pressure before the time of arrival of the reflected wave. The frequency of the disturbance is 730 cps. With a chamber length, measured from the injector face to the sonic plane, equal to 2 ft, the equivalent wavelength would appear to be 4 ft. Therefore, the expected wave velocity relative to the gas would be 2920 fps. This is below the expected speed of sound for liquid oxygen = JP-5A combustion products and is less than the propagation velocity as determined from the transducer outputs in the following manner.

Velocities of wave propagation relative to a stationary observer are determined by dividing the distance between adjacent transducers by the time required for the wave to travel between transducers. The average value of the upstream and downstream velocities of propagation yields the propagation velocity relative to the gas which, in this case, is 3360 fps. Previous analytical work under the contract has shown that the droplet and gas ballistics are consistent with a chamber temperature of 5500°R and a sonic velocity of 3580 fps. Since the temperature and speed of sound are decreasing through the converging portion of the nozzle, the average sonic velocity relative to the gas would be less than 3580 fps.

The apparent anomaly between the wave velocity as determined from the frequency and equivalent wavelength (2920 fps) and the velocity as determined from the upstream and downstream averaging (3360 fps) can be explained by work done previously at the Polytechnic Institute of Brooklyn.[3] It was shown that the resonant frequency for a duct containing a gas flow at some finite Mach number $M$ is given by

$$f_r = c(1 - M^2)/2l \qquad (1)$$

or the equivalent wavelength is

$$\lambda = [2l/(1 - M^2)]$$

where $l$ is the geometrical length of the duct, $c$ is the average

wave velocity relative to the gas, and the duct is assumed to behave as a half-wave resonator. Therefore, the product of the measured frequency and twice the duct length does not yield the average wave velocity, but rather this latter quantity multiplied by a factor of $(1 - M^2)$. For a resonant frequency of 730 cps, a duct length of 2 ft, and an average wave velocity of 3360 fps, the Mach number as determined from the previous equations is 0.367. Since the nozzle entrance Mach number on the motors used in these tests is 0.45, and the duct length includes the convergent portion of the nozzle, the average Mach number as determined from the resonant frequency appears to be reasonable.

It is obvious that for low Mach numbers and large contraction ratios the effect on the resonant frequency is small, but as the Mach number increases, the reduction in natural or resonant frequency increases. If one has a beforehand knowledge of the wave velocity relative to the gas, say 3360 fps, and uses simple acoustic theory ($M = 0$), the resonant frequency for a 2-ft chamber would be 840 cps. As the Mach number is increased to 0.367, a 13% decrease in resonant frequency is noted.

An important conclusion to be derived from the foregoing discussion is that acoustic theories will not give accurate quantitative results of the analysis of wave oscillations in rocket motors, especially those having small contraction ratios with resultant high Mach number profiles.

### References

[1] Burstein, S., Hammer, S., and Agosta, V. D., "Spray combustion model with droplet breakup: analytical and experimental results," *ARS Progress in Astronautics and Rocketry: Detonation and Two-Phase Flow*, edited by S. S. Penner and F. A. Williams (Academic Press, Inc., New York, 1962), Vol. 6, pp. 243–268.

[2] Peschke, W. and Hammer, S., "Pressure gradients in a liquid propellant rocket motor: effect of injector configuration," AIAA J. 2, 1467–1469 (1964).

[3] Agosta, V. D. and Mazzitelli, D. A., "A theoretical study of the vibratory forcing functions in axial flow turbo-jet engines due to flow pulsations," Wright Air Development Center TR 56-74 (January 1956).

# Stagnation Equilibrium Layer in Nonequilibrium Blunt-Body Flows

RAUL J. CONTI*
*Stanford University, Stanford, Calif.*

### Introduction

IN 1962, Swigart[1] introduced a novel technique for analyzing inviscid perfect gas flows over blunt bodies in hypersonic flight. The present investigation makes use of this technique to study nonequilibrium flows, and in this paper attention is drawn to the equilibrium layer that exists near the body. Before pursuing this point any further, a brief discussion of the method is included.

The technique in question has been called the method of successive truncations. Its framework is a scheme of systematic approximations where each approximation is rendered solvable by truncation of infinite series. These series are expansions of the flow variables in powers of the curvilinear coordinate leading away from the axis of symmetry of the flow. Thus, for the plane flow field behind a circular-cylindrical shock, Swigart works with the stream function and density ($\psi$ and $\rho$) which are expanded as (see Fig. 1)

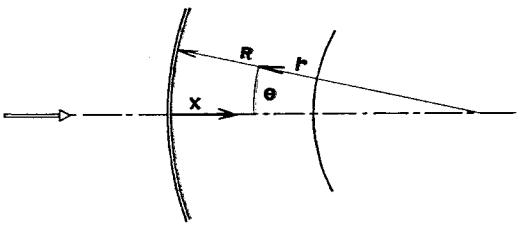


**Fig. 1 Circular-cylindrical coordinate system.**

$$\psi(r,\theta) = \psi_1(r)\sin\theta + \psi_2(r)\sin^3\theta + O(\sin^5\theta) \quad (1a)$$

$$\rho(r,\theta) = \rho_1(r) + \rho_2(r)\sin^2\theta + O(\sin^4\theta) \quad (1b)$$

The assumption is made that this representation for $\psi$ and $\rho$ is valid for all $\theta$ of interest. Then, substitution of the expansions into the governing partial differential equations and equating of like powers of $\sin\theta$ yields sets of ordinary differential equations for the quantities $\psi_i$, $\rho_i$. The first-order set, or first-order problem, is defined by two ordinary differential equations for $\psi_1$, $\rho_1$, and $\rho_2$. The appearance of $\rho_2$ in the first-order problem is due to the ellipticity of the governing partial differential equations and brings about the necessity for some other means of determining $\rho_2$. One such means is truncation of expansions (1) at the first term, i.e., setting $\rho_2 = 0$.† This renders the first-order problem solvable, but also introduces an approximation in the results. A similar situation occurs in higher-order problems, which are also solved by truncation, thereby creating the successive-approximation character of the method in question.

In the method of successive truncations, each truncation level can be regarded as postulating the $\theta$ variation of the flow variables and solving for the $r$ variation. In this light, it is obviously desirable to make a good guess for the $\theta$ variation [i.e., assume the proper form for expansions (1)]. This has the double effect of giving good results locally and extending the $\theta$ range of validity of the particular truncation being solved. It is presently suggested that this is not easy to do when the density is used as a variable, since density is expected to be nearly constant in the immediate vicinity of the shock and to vary as $(\cos\theta)^{2/\gamma}$ near the body according to the Newtonian approximation. It is clear that no single function of $\theta$ will represent the proper density variation both near the shock and near the body. This is perhaps the reason for the poor results exhibited in the first truncation of Ref. 1 for the case at hand (flow behind a circular-cylindrical shock). Here the density behavior at the shock was retained, as can be seen from expansion (1b) in which the first term is independent of $\theta$. On the other hand, a variable that is much more accurately expressible as a function of $r$ times a function of $\theta$ is the pressure, which can be expanded as

$$p(r,\theta) = p_1(r)\cos^2\theta + O(\sin^2\theta) \quad (2)$$

which exhibits the cosinusoidal-square variation that is actually expected both near the shock and near the body in hypersonic flow. It is suggested that the use of expansion (2) rather than (1b), by exploiting a characteristic of the actual flow behavior, sets the basis for a meaningful first truncation to which successive approximations contribute only in a relatively minor way. This situation is not expected to change in the nonequilibrium case, which was then analyzed using the preceding ideas. First-truncation nonequilibrium results are discussed in the remainder of this paper.

Received July 1, 1964. This work is part of an investigation carried out under Air Force contract AF 49(638)1280. The author is indebted to M. D. Van Dyke and H. K. Cheng for their helpful suggestions.

* Research Assistant, Department of Aeronautics and Astronautics.

† An alternative to this is the device used by Kao.[2]